Status Report on the Borexino Muon Identification System

February 29, 1997

L. Oberauer, S. Schönert

on behalf of the TU-München Muon Group

Contents

1 Introduction

Borexino aims for detecting low energy solar neutrinos in a real time experiment. Crucial for the success of the project is a sufficient low background counting rate. Results obtained in an underground Counting Test Facility (CTF) at the Gran Sasso Laboratory showed very promising results about the internal radioactivity of Borexino detector materials. However, the CTF provided also the insight, that the remaining underground flux of cosmic muons may create a non negligible number of signals which cannot be distinguished from neutrino candidates, therefore jeopardizing the experiment. As a conclusion the setup of a muon identification system for Borexino was decided.

2 The Borexino Experiment

2.1 Neutrino Detection in Borexino

The aim of the solar neutrino experiment Borexino is to measure in real time the solar neutrino flux with a low energy threshold and with high statistics and energy resolution via the pure leptonic neutrino electron scattering process $\nu + e^- \rightarrow \nu + e^-$. Target is a liquid scintillator with fiducial mass of ca. 100t.

Motivation for Borexino comes from the long standing solar neutrino puzzle. Data analysis of the existing experiments leads to the assumption of severe suppression of the solar ^7Be-branch, which probably cannot be explained by modifications of the standard astrophysical model of the sun. The monoenergetic ^7Be-neutrinos give rise to a compton like recoil spectrum in Borexino. Its edge will be at 660 keV, significantly higher than the aimed energy threshold of ca. 250 keV. Thus ^7Be-neutrino detection is very efficient in Borexino. Depending on the physical scenarios different signal rates can be expected:

- Assuming validity of the standard model a counting rate for ^7Be-neutrinos, which would consist in this case purely as ν_e, of roughly 55/day in Borexino is expected.
- In scenarios of total neutrino flavour conversion (i.e. for neutrino mass differences $\Delta m^2 \approx 10^{-6} \rightarrow 10^{-5}\ eV^2$) a reduced flux down to approximately 12/day would be measured due to the lower cross section of $\nu_{\mu,\tau}$ scattering, which occurs only via neutral current interaction.
- In case of vacuum oscillations (i.e. for neutrino mass differences $\Delta m^2 \approx 10^{-10}\ eV^2$) Borexino would see a distinct time dependent periodical neutrino signal due to the seasonal eccentricity of the earth's orbit around the sun.
- For neutrino mass differences in the range of $\Delta m^2 \approx 10^{-7}\ eV^2$ and for large mixing Borexino should see a 'day/night' effect due to electron neutrino recovery during the path through the earth.

If Borexino is successful the measured ^7Be-flux can be compared with results from experiments using charge current reactions exclusively. These results may come from radiochemical measurements, but also from future real time experiments as it was proposed recently [1]. Total conversion of ^7Be ν_e to $\nu_{\mu,\tau}$ would mean no signal in charged current experiments and a reduced signal in Borexino, demonstrating neutrino flavour conversion uniquely.

Borexino also can serve for additional projects in neutrino physics. Search for a magnetic moment can be performed by means of terrestial neutrino sources by investigating the electron recoil shape at low momentum transfer. Via the inverse beta-decay $\bar{\nu_e} + p \rightarrow e^+ + n$ Borexino can look for signals from geophysical neutrinos [2, 3] as well as for neutrinos emitted by european nuclear power plants [4]. The latter would serve as a long baseline neutrino oscillation experiment probing the so-called large mixing angle solution for the solar neutrino problem.

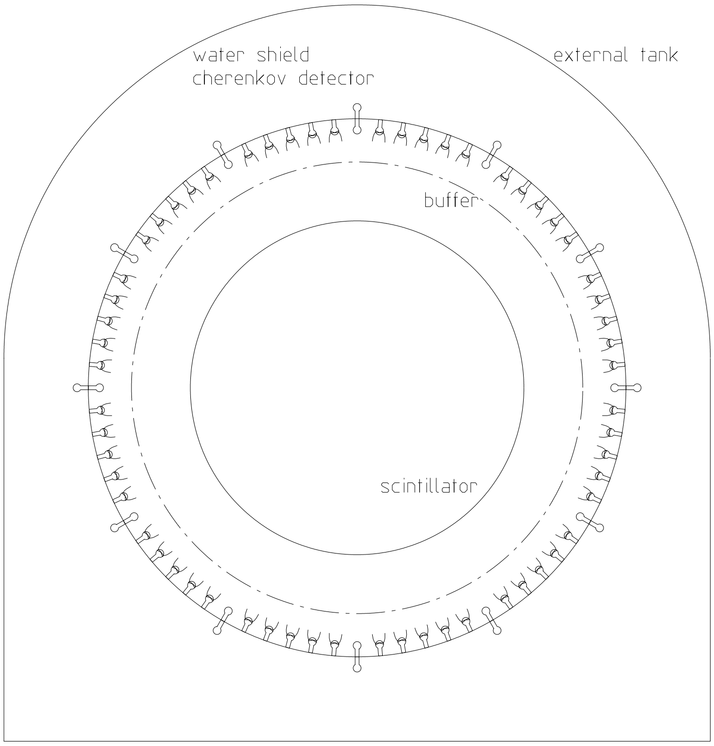

Figure 1: *Schematic view of Borexino. The ultrapure scintillator (300t) inside a nylon vessel is shielded differentially by means of a liquid buffer (1040t), a steel sphere on which the tubes are mounted, and the outer water buffer which is contained in an external steel tank (diameter and height ca. 18m). A transparent nylon shroud hinders radon convection in the liquid buffer region. Additional tubes mounted on the outer surface of the steel sphere allow detection of penetrating muons via the Cherenkov effect. Each 6th of the inner tubes has no light guide, which enhances the acceptance of Cherenkov photons arising from muons intersecting the liquid buffer. This allows further muon identification. For explanation see text.*

2.2 The Detector and general Background Considerations

The detector is shielded successively from outer radioactivity by means of an onion-like structure. Here the adjacent inner layer serves as shielding and has to provide an increased purity in terms of internal radioactivity. Fig. 1 shows the experimental setup.

Borexino is placed in hall C of the underground laboratory at Gran Sasso, Italy. An overburden of ca. 3500 m.w.e. suppresses the cosmic muon flux to 1.1 $/hm^2$ and shifts the mean energy of the muons to 280 GeV. The outer part of the detector consists of a steel tank with 18m in height and diameter. Inside this 'external' tank a stainless steel sphere will support 2240 phototubes on the inside and 208 tubes at the outside. The steel is treated via an electropolishing procedure in such a way that the reflection of photons is suppressed. Most of the tubes inside the sphere will be equipped with light guides in order to increase the geometrical coverage and hence the energy resolution. Between external tank and sphere high purity water will serve as shielding against external gamma rays and as an active Cherenkov counter tagging penetrating cosmic muons[1]. The steel sphere will be filled with a transparent, high purity buffer liquid which itself holds a nylon sphere, filled with organic scintillator. Between the steel sphere and the scintillator region an additional nylon shroud hinders radon convection from the outer area towards the critical region.

The active scintillator mass will be around 300t. By means of time of flight measurements the event position can be reconstructed and a fiducial volume for solar neutrino interaction defined. Latter should be about 100t, establishing a counting rate of 55 neutrinos per day according to the standard solar model. The outer part of the scintillator sphere serves as active shielding.

The demands on purity in terms of radioactivity in Borexino, especially for the scintillator itself, are challenging. In order to be able to extract a clear signal from background events also in case of total flavour conversion, an intrinsic concentration in Uranium and Thorium of ca. 10^{-16} should not be exceeded significantly. The amount of $^{14}C/^{12}C$ must not be higher than $\approx 10^{-18}$. In order to test scintillating materials a large Counting Test Facility (CTF) has been built up in hall C of the underground laboratory at Gran Sasso, which resembles a small prototype (ca. 5t of scintillator) of Borexino. From beginning of 1995 until summer 1997 several tests about the feasibility of Borexino including procedures to maintain the purity of the scintillator have been performed, which showed encouraging results: $^{14}C/^{12}C = 1.94 \cdot 10^{-18}$, $^{238}U = (3.5 \pm 1.3) \cdot 10^{-16}\ g/g$, $^{232}Th = (4.4 \pm 1.5) \cdot 10^{-16}\ g/g$. A complete discussion of the CTF results including experimental techniques for further background suppression are given in [5] and [6]. Details about the experimental setup of the CTF can be found in [7].

Highly developed neutron activation analysis (NAA) of scintillation samples performed in Munich is now sensitive in the same regime, providing an independent test on the radiopurity and allowing tests on the secular equilibrium of the decay chains. With NAA an upper limit for uranium of $^{238}U < 2 \cdot 10^{-16}\ g/g$ (90% CL) has been obtained. In addition concentration values or limits have been measured by this method for various isotopes, including man-made nuclei for different detector materials. For details, see [8].

---

[1] The Outer Detector as described in Section 4.

Detector part	muon intersection rate (counts per day)
Inner vessel	2025
Steel sphere	5150
External tank	9900

Table 1: *Muon intersection rate for different parts of the Borexino detector.*

2.3 Muon background rates, CTF results

In calculating the muon rate expected for Borexino, we took the zenith muon distribution measured by the Macro collaboration at Gran Sasso and for the absolute normalization the experimental obtained value of 1.1 muon per hour and square meter. Tab. 1 shows the muon intersection rates for different parts of our detector.

About 10^4 muons per day hit the detector. Since the neutrino interaction rate will be in the range of a few counts per day in scenarios of full MSW-conversion, the overall muon leaking ratio into the neutrino window after all cuts must not exceed a value of about 10^{-4}.

Muon events inside the inner vessel will create pulses far above the solar neutrino spectrum. However, muons with tracks just between the steel sphere and the inner vessel may create signals just in the relevant energy region. According to Tab. 1 the rate of these muons is expected to be around $3 \cdot 10^3$ per day.

Since the timing of muon pulses should be different when comparing beta events, software cuts provide a tool to separate muons from neutrino candidates. In the CTF this was tested experimentally by means of a muon telescope installed on top of the CTF tank. Two position sensitive MWPC chambers with $3.42\,m^2$ sensitive area were installed and data taking occurred from August 1995 until end of 1996. Coincidences with the CTF showed that 24% of all muons intersecting the CTF water tank produce signals which are in the neutrino window between 250 keV and 800 keV. By measuring the meantime of the individual PM signals and comparing it to beta pulses (e.g. from the alpha beta delayed coincidences occurring in the radium chain) only 1.6% of all muons remain good candidates and have pulse heights within the neutrino window. However, this rejection factor still would be to small in Borexino.

The dimensions and the buffer material will be different in Borexino and from calculations one can expect better separation values (e.g. Section 5). However, these calculations certainly do not include possible "pathological" events which occur rarely, but can be of relevance in a low counting rate experiment as Borexino. For instance high energetic neutrons may enter the inner detector, even when the muon intersects the buffer region only. Without a hardware muon veto system those events could not be tagged.

There is hope in developing processes which might even improve the performance in purifying liquid scintillators. In this case, if no hardware muon veto system exists, the muon generated background would become dominating and condemn those developments as meaningless.

To base muon identification on software analysis alone would therefore be unreasonable. In addition such a method depends crucially on a reliable method to study systematic uncertainties. A hardware muon identification system would provide this method, because any possible software cut can be "calibrated" by the muon veto system. The rejection power as well as the acceptance for good events can then be determined experimentally. In Section 4, "Outer Detector", muon identification via the external Cherenkov detector is described quantitatively.

In addition a hardware muon identification system will provide a diagnostic tool for cosmogenic created nuclei with moderate long lifetimes as ^{11}C. It has the potential to define the spatial correlation between the muon track, the vertex of the shower creation, the location of neutron capture and of the delayed decay of produced radio isotopes. Though the possibility of muon track determination is not a primary objective of the Muon Identification System, it is considered to be a desirable feature of the system.

In a separate experiment we have recently measured the effective cross sections of radio isotope production in muon induced showers. Moreover, the activation profiles, i.e. the lateral probability distributions from the muon track have been determined. These results are reported in Section 6.

We conclude that the CTF results and calculations on the muon rates in Borexino demand the set up of a high efficient muon identification system which must not be based on software tools solely.

3 Strategy of the Muon Identification System

Careful analysis of the CTF-data clearly showed the necessity of an active muon identification system for Borexino. As discussed in the former section the leaking rate should not exceed a level of $\approx 10^{-4}$. This only can be achieved by a system based on several pillars. Our 'sub-systems' are:

- The *Outer Detector*: It will be a water Cherenkov detector, consisting of 208 photomultiplier (PMs) mounted on the outer surface of the steel sphere. We take advantage of the pure water shielding of Borexino. The Outer Detector is described in Section 4. Muons intersecting the water tank should be identified with high efficiency $>$ 95%.
- The *Inner Detector*: 2240 PMs are homogeneously distributed with 1866 of them equipped with light guides. Therefore about 16.7% of the tubes accept photons from all directions whereas PMs with light guides do accept photons mainly from the scintillator region. Cherenkov photons created along the track of the muon in the buffer liquid have a higher efficiency to hit a PM without light guide. Therefore, comparing the sum of photoelectrons from these tubes without light guides with the total sum of photoelectrons allows to separate between muon events and events from the scintillator. The Inner Detector is described in Section 5. Its separation efficiency of the Inner Detector should be $>$ 95%.
- The *Offline Analysis*: In analyzing the CTF data we have found several strategies to discriminate between beta- and muon events. Most of them are based on the unique timing distribution in the signal of a muon. Due to the different geometric situations these results cannot be fully adopted to the Borexino case. However, we have tested these strategies in Monte-Carlo calculations and found them to be sensitive also in Borexino. A description of these methods can be found in Section 5. The cut efficiency should be $>$ 95%.

These 'sub-systems' can be tested and calibrated mutually, thereby reducing systematic errors. This is, besides a combined identification efficiency of $\approx 10^{-4}$, an essential advantage of dividing the muon veto system in different parts.

Cosmogenic generated background due to muon interaction with nuclei from the detector material is discussed in Section 6.

4 Outer Detector (OD)

The region between the Outer Steel Tank (OST, volume 3500 m^3) and the Stainless Steel Sphere (SSS, diameter 13.70 m, volume 1350 m^3) is filled with 2150 m^3 of water. About 208 8" PM (EMI 9531) are mounted on the surface of the SSS viewing the water buffer. This part of the Borexino detector is named the Outer Detector (OD). The water buffer of the OD serves two functions: it shields (passively) against low-energy ambient radioactivity as gamma rays and neutrons coming from the rocks, and it provides an active water Cherenkov detection system for high energetic cosmic muons and their secondaries.

The PM surface density on the SSS amounts to 208 PM per 580 m^2, i.e. about 1 PM per 2.8 m^2. Two adjacent PMs are separated by a distance of typically 1.7 m. The shortest track length between OST and SSS is 2.15 m. The inner surface of the OST and the outer surface of the SSS are covered with 0.2 mm thick Tyvek plastic sheets. Tyvek is a white polyolefin plastic with a diffuse reflectivity of over 90% for visible light. The spectral reflectivity has been measured and is displayed in Fig. 2 together with the PM quantum efficiency and the primary photon spectrum. Cherenkov photons can impinge either directly on the photomultiplier cathode or after (several) reflections from the Tyvek film. The diffuse character of the reflection distributes the photons over a large surface area and hence increases the overall photoelectron (pe) yield as well as the number of triggered PMs.

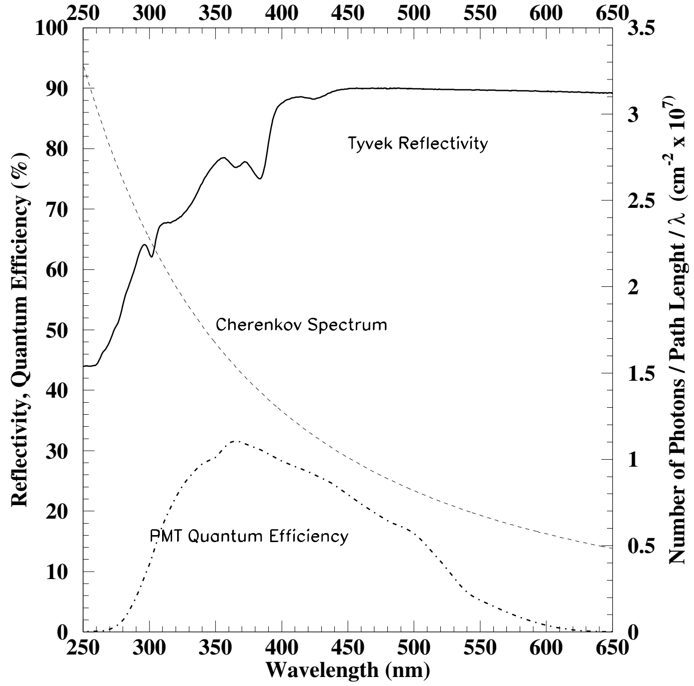

Figure 2: *The spectral reflectivity of a 0.2 mm Tyvek plastic sheet is displayed together with the EMI 9351 Photo-cathode efficiency and the primary muon Cherenkov spectrum.*

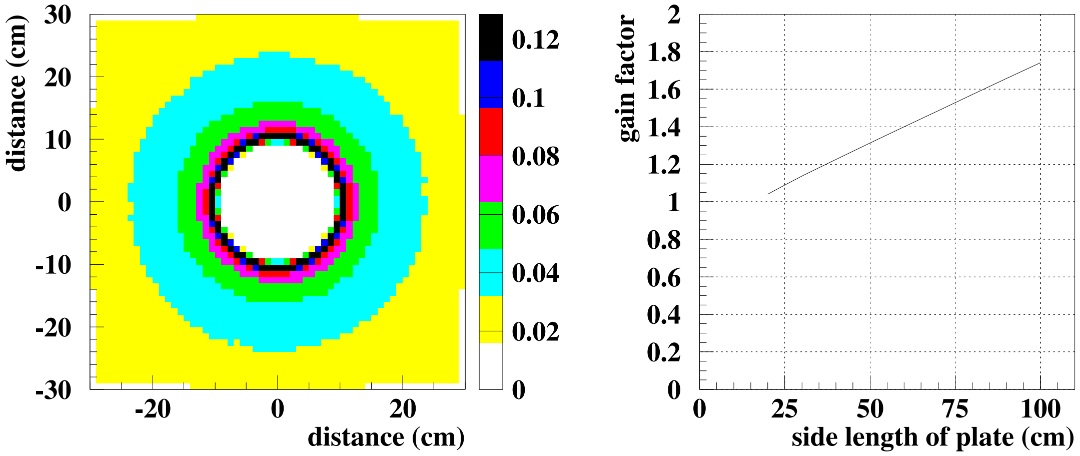

Figure 3: *The left plot shows a simulation of the response of a 60 cm x 60 cm wave shifter plate. The color code reflects the probability that a photon which impinges on the panel is being transported to the PM. In the right plot, the photo electron gain is shown as a function of to the side length of the wave shifter panel. A uniform illumination is assumed which however is* **not** *the case in a Cherenkov cone.*

Optionally, the PMs will be equipped with wavelength shifter panels in order to further increase the pe-yield and the number of triggered PMs [9]. A wave shifter panel consists of an acrylic sheet of dimensions 60 cm x 60 cm x 1.3 cm which is doped at a concentration of 50 mg/l with bis-MSB (p-bis(0-methyl styryl) benzene, $C_{24}H_{22}$). The panel has a circular hole in its center for mounting a PM.

Photons which impinge on a wave shifter panel can be absorbed and remitted by the bis-MSB and guided via total internal reflection to the PM cathode. A quantitative model of the wave shifter panel is shown in Fig. 3.

The overall OD design is inspired by the Super-Kamiokande muon veto system. Many details on materials as well as on detector performance have been obtained from the BU Super-K group which we would like to acknowledge. The main difference between the Super-K and Borexino OD is that Borexino has a spherical symmetry with a relative smaller radius. It appears that this is favorable for the distribution of light over a wide surface area. This has an impact on the pe-yield and on the number of triggered PMs.

4.1 Mechanical Design for OD PMs

The PM encapsulation and sealing used in the OD are identical to the one used in the ID. In addition it is planed to use a teflon heat shrinking tube glued to the steel housing and glass of the PM. A sketch of the design is shown in Fig. 4. The mu-metal shield is reduced with respect to the design of the ID-PMs, however measurements have shown that the pe collection efficiency does not decrease more than 10% for a ‘worst case magnetic field direction’ in Borexino.

Figure 4: *Sketch of a PM of the OD including mu-metal shielding and wave panel shifter plate.*

4.2 Trigger Conditions and DAQ for the OD

It is planned to read out the OD signal under the conditions a) when both ID and OD give a trigger signal simultaneously, b) when a trigger is generated in the OD only and no trigger in the ID, and c) when the ID is triggered and no trigger is generated in the OD simultaneously. The condition a) aims at an event class when muons intersect both OD and ID. Condition b) points at the rarer case that a muon track does not intersect the ID but its secondaries (e.g. neutrons) create radioactive isotopes inside the SSS which consecutively decays and generates a correlated delayed signal. The purpose of condition c) is to recognize events which create a sub-threshold signal in the OD and trigger signal in the ID (e.g. high energy neutrons penetrating the OD).

It is planned to use the Borexino standard electronics developed by the Genova group [10] with a dynamic range from 1 – 30 photo-electrons (pe) per channel. An OD trigger is created by a given PM hit-multiplicity within a time window of about 100 nsec in combination with the total collected charge. This provides efficient discrimination against gamma ray background signals and random coincidences. Both charge and timing of each PM is recorded for the off-line analysis.

4.3 Performance of the OD - Monte Carlo Simulation

The Monte Carlo Code **MU**on **CER**erenkov **T**racker (**MUCERT**) has been developed in order to simulate the response of the OD with respect to Cherenkov photons generated by high energetic muons or electrons. It is designed to be interfaced with EGS or GEANT which provide the input data of the shower generating and propagation. **MUCERT** then tracks the emitted Cherenkov photons through the detector until they create a signal in a PM or are absorbed without signal generation. The code contains the full detector geometry, the physics of light propagation, i.e. scattering, absorbtion and reflection of surfaces, and the response of the PM and wavelength shifter panels.

Some of the results of the simulations will be subsequently discussed in order to characterize the performance of the OD. In particular, the response of the OD has been evaluated for various detector configurations, i.e. changing reflectivities of the surface materials, with and without waveshifter panels and with different PM surface densities. Moreover, the effect of PM failures on the detection efficiency as well as the problem of light shadowing of support structures and PM cables were investigated. Preselected muon impact parameters were simulated in order to test 'worst case' scenarios.

4.3.1 Effect of Surface Reflectivity and of Waveshifter Panels

In Tab. 2 the photo-electron (pe) yield and the number of firing PMs per muon interaction is displayed as a function of the integral surface reflectivity. A high reflectivity increases both significantly the number of hit PMs and the overall collected charge (pe-yield). With a Tyvek plastic surface coverage (cf. Fig. 2) the integral reflectivity corresponds to about 80% in the spectral range of interest.

reflectivity	pe-yield	no. of PM hits
0.0	64	4
0.2	92	20
0.4	129	37
0.6	210	64
0.8	445	126
0.9	904	185

Table 2: *Monte Carlo simulation of the total photo-electron (pe) yield and of the number of triggered PMs for various surface reflectivities assuming diffuse reflection. No wave shifter panels are included in this simulation. 208 PMs are distributed with equally spaced over the surface of the SSS. The numbers are based on the simulation of 1000 muon each passing through the buffer between SSS and IV.*

The impact of waveshifter panels on the pe-yield and firing PMs is shown in Tab. 3. Fig. 5 depicts the distribution of collected photo electrons (N.B. no saturation of the electronic was assumed) and of the number of triggered PMs for muons passing through the buffer. The main effect of the panels is the total increase of the pe-yield.

	pe-yield	no. of PM hits
with shifter panels	564	132
without shifter panels	446	126

Table 3: *Monte Carlo simulation of the total photo-electron (pe) yield and of the number of triggered PMs with and without waveshifter panels. The gain in collected charge (pe-yield) is about 26% while the increase in the number of triggered PMs is about 5%. An integral surface reflectivity of 80% was assumed and a muon sample was selected which intersects the buffer area (in between IV and SSS).*

It is noteworthy that the pe's are *not* equally distributed on the triggered PMs. It occurs that there are 'hot-spots' close to the intersection points of the muon track with the SSS with a high pe density. Up to several hundred pe's are being detected by one or two PMs while adjacent PMs collect typically about 10 pe (without waveshifter panels). PMs at larger distances from the intersection points give signals at the single pe level. Fig. 6 shows a Monte Carlo event of a muon crossing the OD along the central vertical axis. A muon penetrating the OD in between the SSS and OST is displayed in Fig. 7. The color code of the PMs indicate the time of arrival of the first pe and the size of the squares the pe-yield.

4.3.2 Effect of the Muon Track on the OD Response

Owing to the spherical geometry of the detector, the muon track length changes with the impact parameter (δ), i.e. the shortest distance of the muon track from the center of the detector. Consequently the pe-yield is expected to increase with increasing δ. The minimal pe-yield and number of fired PMs occurs when the muon track intersects the SSS radially and the maximal when the track passes vertically through the space between the SSS and OST. One can subdivide δ in three classes:

- a muon is intersecting the IV, i.e. $\delta < 4.25$ m,
- a muon is crossing in between the IV and the SSS, i.e. $4.25 < \delta < 6.80$ m,
- a muon is crossing in between the SSS and the OST, i.e. $6.80 < \delta < 9.0$ m.

The values of the collected charge and the number of firing PMs are listed for the three cases in Tab. 4.

4.3.3 Effect of PM Failures on the OD Response

During the time of data taking one has to expect that a certain PM mortality occurs. Though the OD is in principle accessible *without* emptying the ID and broken PMs are replaceable, it is not foreseen to access the OD on a regular basis. Therefore, the number of PMs is designed to allow a 20% failure rate within several years. Tab. 5 shows the pe-yield and number of PM hits for a PM failure fraction of 20%. For this purpose, a

impact parameter δ	pe-yield	no. of PM hits
$\delta < 4.25$ m	262	90
$4.25 < \delta < 6.80$ m	445	126
$6.80 < \delta < 9.0$ m	694	149

Table 4: *Monte Carlo simulation of the total photo-electron (pe) yield and of the number of triggered PMs for various minimal muon track distances from the center of the detector (impact parameter δ). The first case corresponds to muons intersecting the IV, the second corresponds to the case that a muon crosses the buffer between IV and SSS and the last case to muons passing through OD only.*

	pe-yield	no. of PM hits
without panels	356	101
with panels	479	120

Table 5: *Monte Carlo simulation of the total photo-electron (pe) yield and of the number of triggered PMs under the assumption that 20% of the PMs are not operational. A subset of muon trajectories was selected which randomly intersect the buffer region (in between IV and SSS). Two detector configurations are compared in the simulation: with and without wave shifter panels.*

given number of PMs was randomly switched off under varying configurations. In Fig. 8 the distributions of detected photo electrons and number of triggered PMs are displayed for a detector configuration with and without wave shifter panels.

4.3.4 Effect of Light Obstruction

The results shown above have been performed in an *ideal* detector geometry; i.e. no structural elements were obstructing light propagation in the OD. This obviously is not the case for the real detector. The main structural elements in the OD are the columns which sustain the SSS and the PM cables. In order to minimize the impact of these objects on the light propagation, all surfaces of these elements will be covered with a Tyvek layer.

In the current design 20 columns with a diameter of 30 cm are attached *vertically* at the equator belt of the SSS. The PM cables will cross the OD *radially* in bundles of about 50 cables inside rigid tubes of about 30 cm diameter. Muons which penetrate along the axis of such a cable tube are *not* visible in the adjacent part of the OD. Due to the radial trajectory however, the muon will intersect the scintillator inside the IV and hence will be recognizable due to the high photon yield. In addition, if the muon crosses the detector, it will provide a signal at the exit point of the SSS. The obstruction of stray Cherenkov photons by the radial tubing has been found to be negligible.

As a worst case scenario for light obstruction one can consider a muon trajectory which intersects vertically at the equator a SSS support column. No light is then emitted in the OD south of the SSS equator. The number of photo electrons in this case is 391 and the number of triggered PMs 106 while Muons with same trajectories however not passing through a column generate 845 pe's and 157 triggered PMs. About half of the light is lost. Owing to the long path length of the muon in the OD for this particular trajectory, the remaining signal is considered to be sufficient. Fig 9 shows the pe-yield and the number of fired PMs for these muon paths.

4.4 Determination of the Muon Track with the OD

The OD signal provides information on the spatial position of the muon track and on the direction of flight. Simple cases as displayed in Fig. 6 suggest that the track position can be reconstructed from the entry and exit point of the 'hot-spots'. The directionality can be deduced from the timing difference: the PM cluster at the exit point of the SSS fires typically about 60 nsec after the PM cluster at the entry point. Muon tracks which traverse the buffer region or the OD without intersection of the SSS are more difficult to reconstruct.

For the future, it is planned to develop a muon track reconstruction program, both for the OD and ID in order to determine the path of flight for all impact parameters of interest.

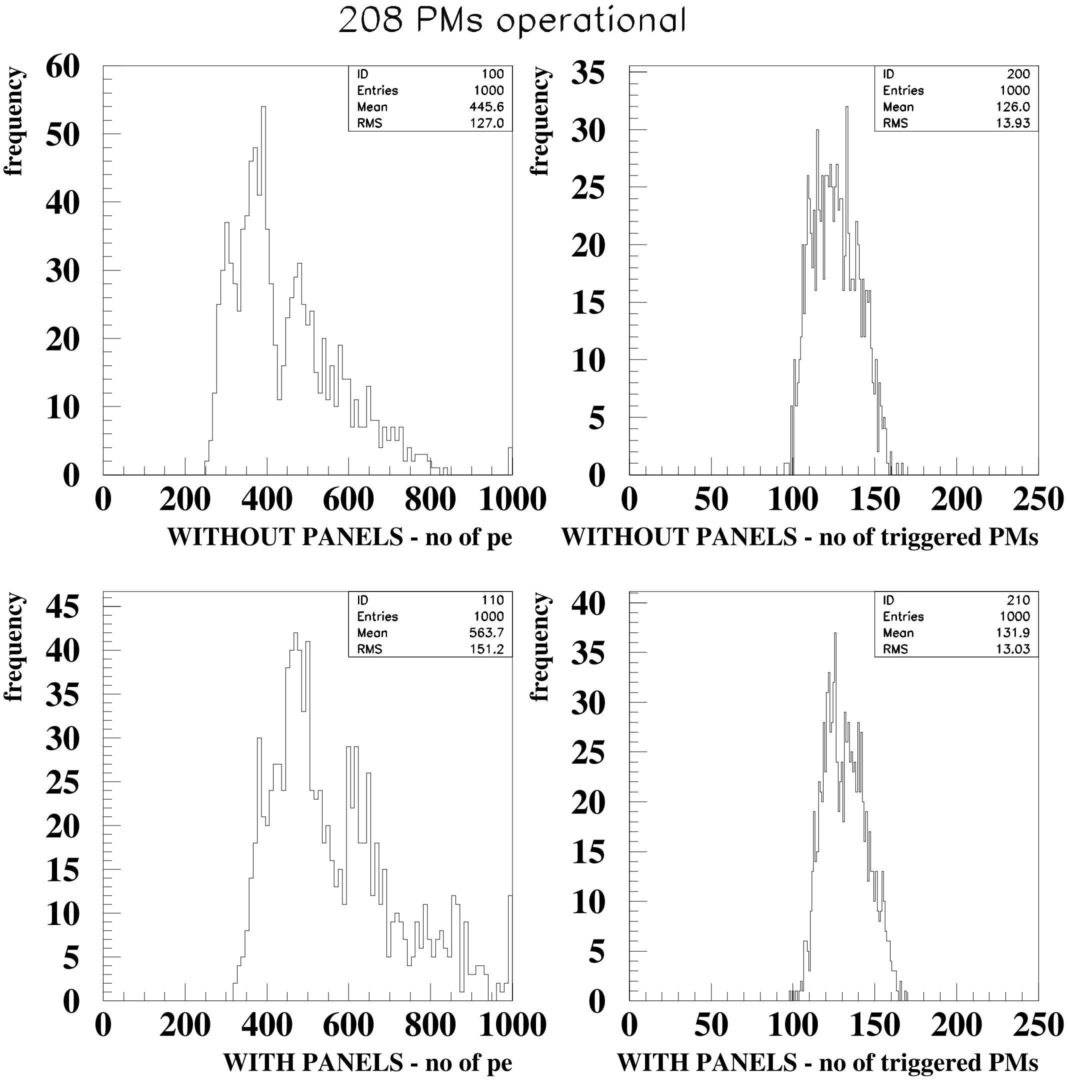

Figure 5: *Distributions of the photo electron (pe) yield and number of fired PMs. In each simulation 1000 muon events were generated to penetrate vertically the buffer region of the detector, i.e. in between the Inner Vessel and SSS. The upper two histograms depict the distribution* **without** *wave shifter panels and the lower two* **with** *panels. An increase of 26% in the pe-yield of 5% in number of triggered PMs is observed.*

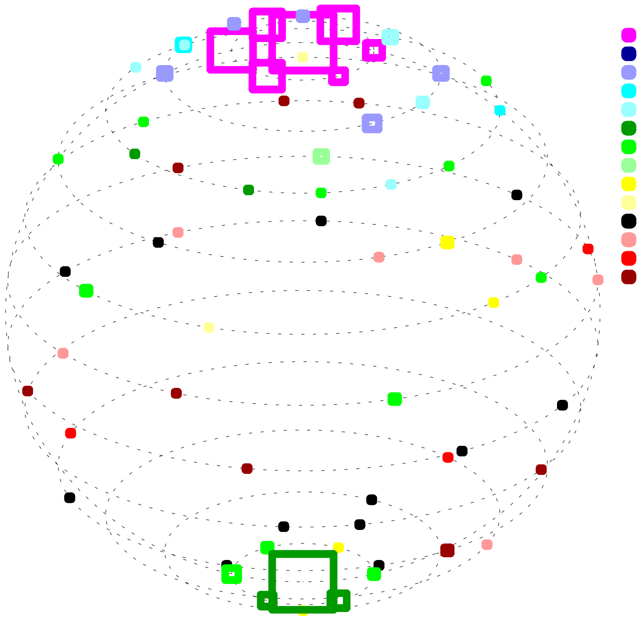

Figure 6: *Monte Carlo event of a muon intersecting the OD along the vertical symmetry axis. The size of the squares correspond to the number of detected pe's and the color code characterizes the time of arrival of the photon. The top PM sees about 470 pe (the size of this square is off scale) and the PMs of the first circle detect about 10 pe each. The color binning corresponds to 10 nsec, thus the time delay between the entry point and the exit point of the muon (hot-spots) correspond to about 60 nsec.*

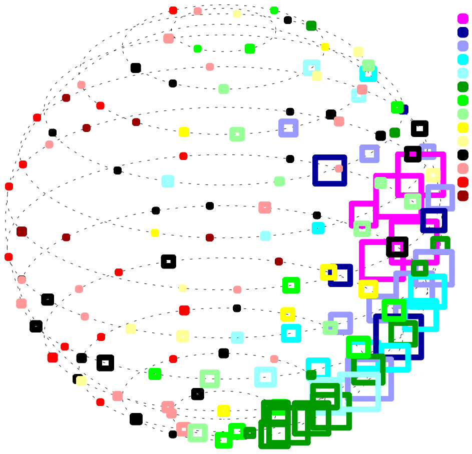

Figure 7: *Here, a Monte Carlo event is shown where a muon passes vertically in between the Stainless Steel Sphere (SSS) and Outer Steel Tank (OST).*

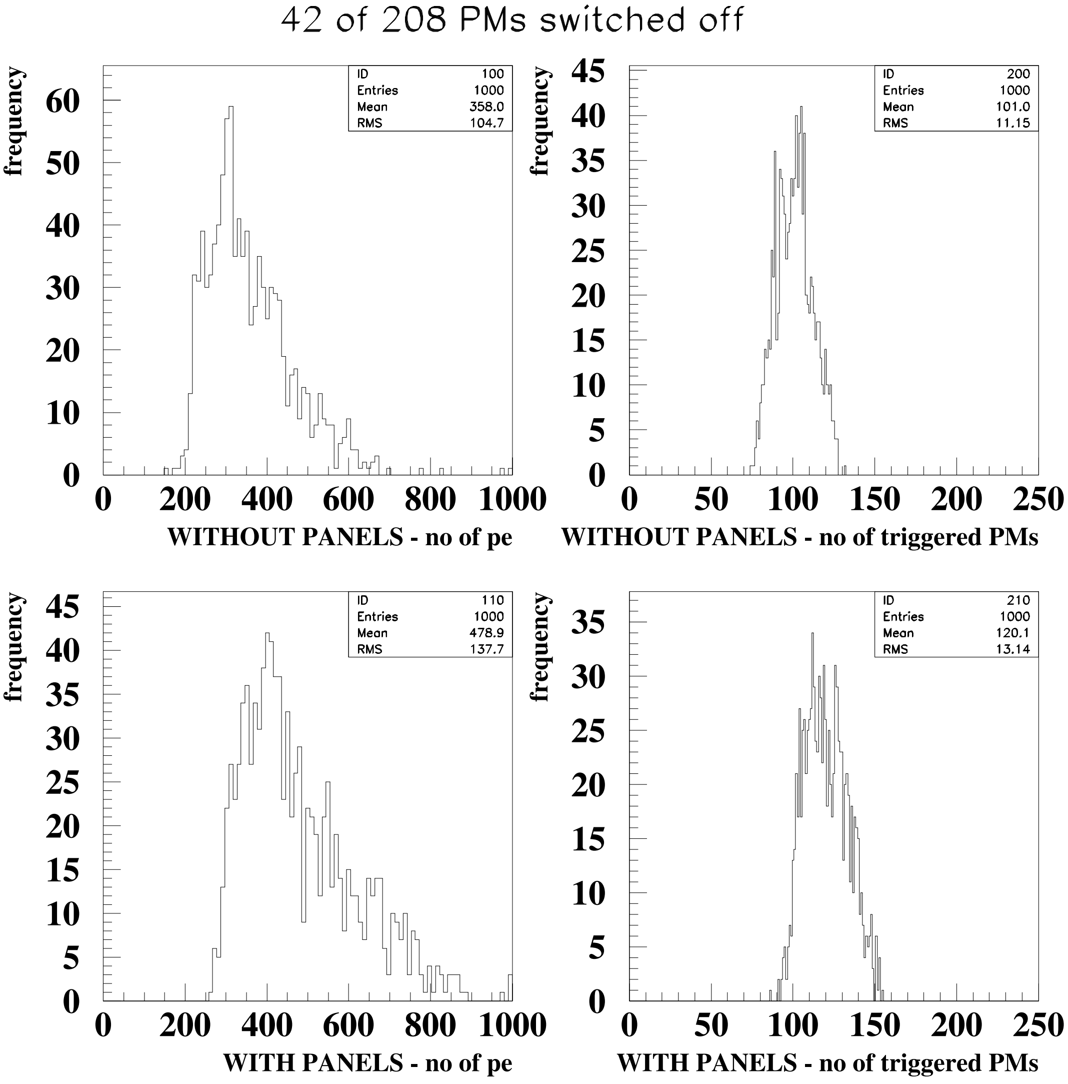

Figure 8: *Distributions of the photo electron (pe) yield and number of fired PMs for 166 operational PMs (20% PM failure). In each simulation 1000 muon events were generated to penetrate vertically the buffer region of the detector. The upper two histograms depict the distribution* **without** *wave shifter panels and the lower two* **with** *panels. An increase of 35% in the pe-yield of 19% in number of triggered PMs is observed for a configuration with panels with respect to a configuration without.*

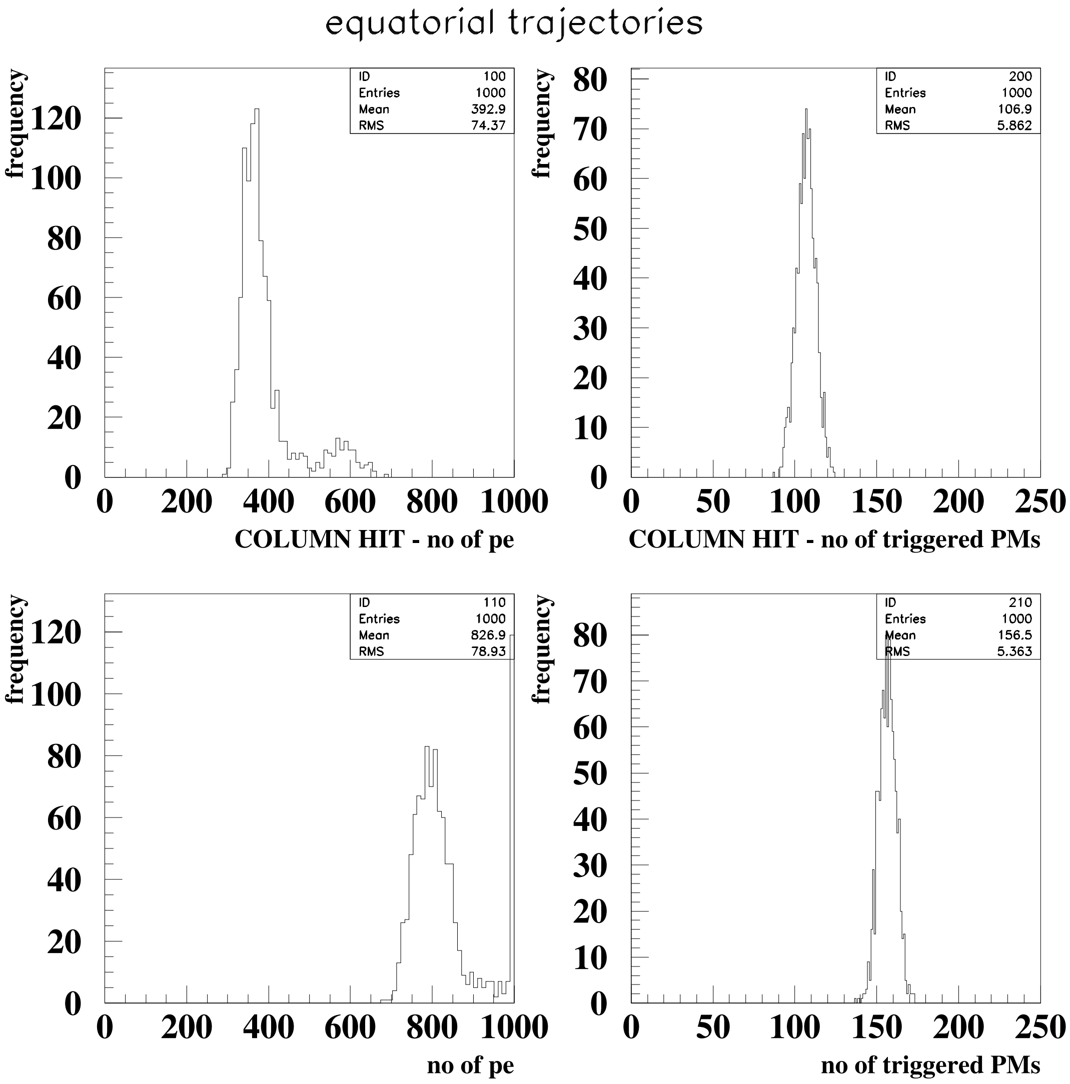

Figure 9: *Distributions of the photo electron (pe) yield and number of fired PMs for Muons crossing the OD vertically on a tangent to the SSS equator. The left plots show muon trajectories which cross along a support pillar. For these trajectories there is no Cherenkov light emission in the lower part of the OD. Though these muon paths have a low probability to occur, the light yield is sufficiently high owing to the long path length in the upper hemisphere.*

5 Inner Detector (ID)

The Inner Detector is contained within a stainless steel sphere of 13.7m diameter. On the surface of the sphere 2240 tubes are mounted. The steel sphere holds the liquid buffer, a nylon shroud which hinders radon convection from the outer region towards the scintillator, and the nylon sphere which contains 300t of ultrapure scintillator.

Cosmic muons traversing the ID create Cherenkov as well as scintillation photons along their tracks. In case the muon hits the scintillator vessel the amount of photons is huge enough to saturate most of the PMs. Hence, these muons are easy to identify. Part of the Cherenkov photons may directly give rise to a signal in the PMs, part of them may be absorbed in the scintillator and be reemitted Stokes shifted in the wavelength, i.e. appearing like scintillation photons. In case the liquid buffer is the solvent of the scintillator, as it is first option in Borexino,[2] muons also will create scintillation photons in the buffer, with their typical emission spectrum which differs from the PC/PPO solution significantly.

A Monte-Carlo code has been written to optimize the detector in distinguishing between muon events in the buffer and beta signals from the scintillator under the precondition not to decrease energy and position resolution capabilities. The program includes Cherenkov and scintillation photon tracking. Input data for the optical model come from measurements performed in Perugia, Milano, and Princeton. The presence of a quencher in the buffer region was assumed, which reduces the scintillation probability in the pure PC liquid and thereby suppresses gamma background events from the steel and the material of the tubes. In the program each photon is tracked. Absorption and diffuse reflection of the steel sphere after the darkening process have been measured in Munich and are taken into account in the code. The performance of the optical light guides in all details has been incorporated fully. Similar programs have been developed in the groups of Milano and Princeton.

The pulse height of muon events, even in the buffer region, is high compared to events in the ^{7}Be-neutrino window. Fig. 10 shows the distribution of registered photoelectrons as function of the least distance ('impact parameter') of the muon track to the center of the detector as calculated in the Monte-Carlo code. Only muons with tracks quite close to the surface of the steel sphere create signals with pulse heights in the region below ca. 1 MeV. Therefore it is essential to identify muons with these impact parameters as efficient as possible.

The numbers of photons and also their probability to scatter and/or to be absorbed depend on the choice of the liquids which are going to be used in Borexino. However, as it turns out in Monte-Carlo calculations some features remain quite stable even when changing some parameter in the optical model. Fig. 11 shows the detector response on a muon intersecting the buffer region of the Inner Detector quite close to the steel surface. Shown are those PMs which registered at least one photoelectron. The colour code is used to give a picture on the timing of such a signal. The timing of each individual channel is determined by the very first photon registered and is depicted in Fig. 11.

---

[2] First option in Borexino is PC/PPO as the scintillator cocktail at 0.15% PPO concentration and PC without PPO as buffer liquid.

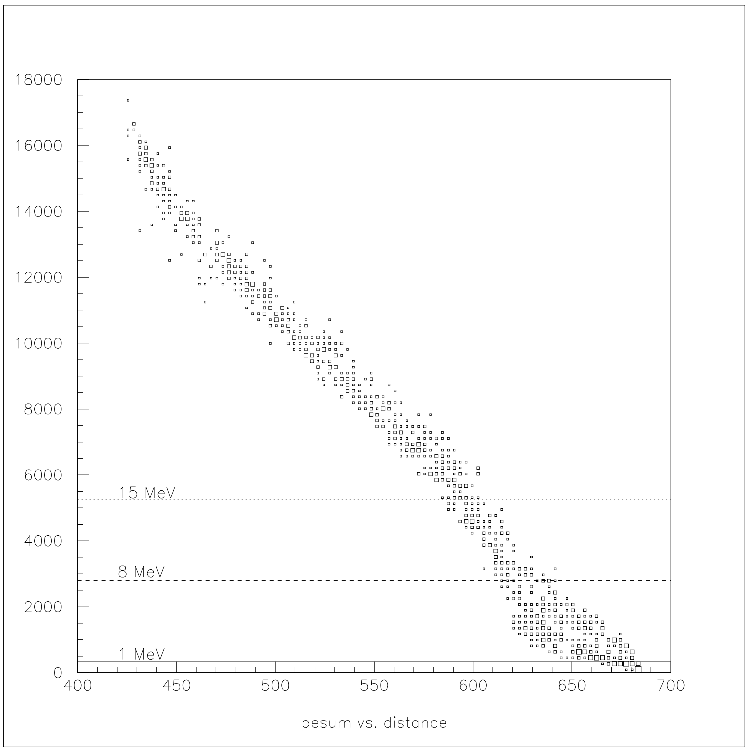

Figure 10: *Distribution of the accepted sum of photoelectrons as function of the distance (in cm) of the muon track to the center of the detector. Dashed lines indicate the number of photoelectrons arising in beta events in the scintillator sphere.*

The size of each individual PM scales with the pulse height.

The timing of muon induced events in the buffer is determined by a fast signal due to scintillation photons and by a retarded component arising from Cherenkov light which is accepted by PMs with light guides on the lower hemisphere (red spots). These photons seem to stem from the scintillator sphere, and hence are accepted with high efficiency even by PMs equipped with light guides. Only the part of photons with wavelength larger than about 430nm contribute significantly to these signals. However, this part is not negligible and shifts the mean time of arriving photons in the region of 50ns to 60ns measured from the very first registered pulse. This is a significant difference to beta-like events from the scintillator sphere and this difference is fairly insensitive to changes in the optical model, because in any case the attenuation length of photons with wavelengths above 430nm has to be large against the dimensions of the detector. Fig. 12 shows the mean time distribution of muon- and beta events, demonstrating the capability to separate between them clearly. The stability of this cut was tested also by 'switching off' PMs in the code. Even at a condition of only 50% of working tubes this simple cut still provides a sensitive separation between beta and muon events.

Most of the tubes, namely 1866, are equipped with light guides in order to increase the optical coverage of the detector. The light guides accept photons coming from the

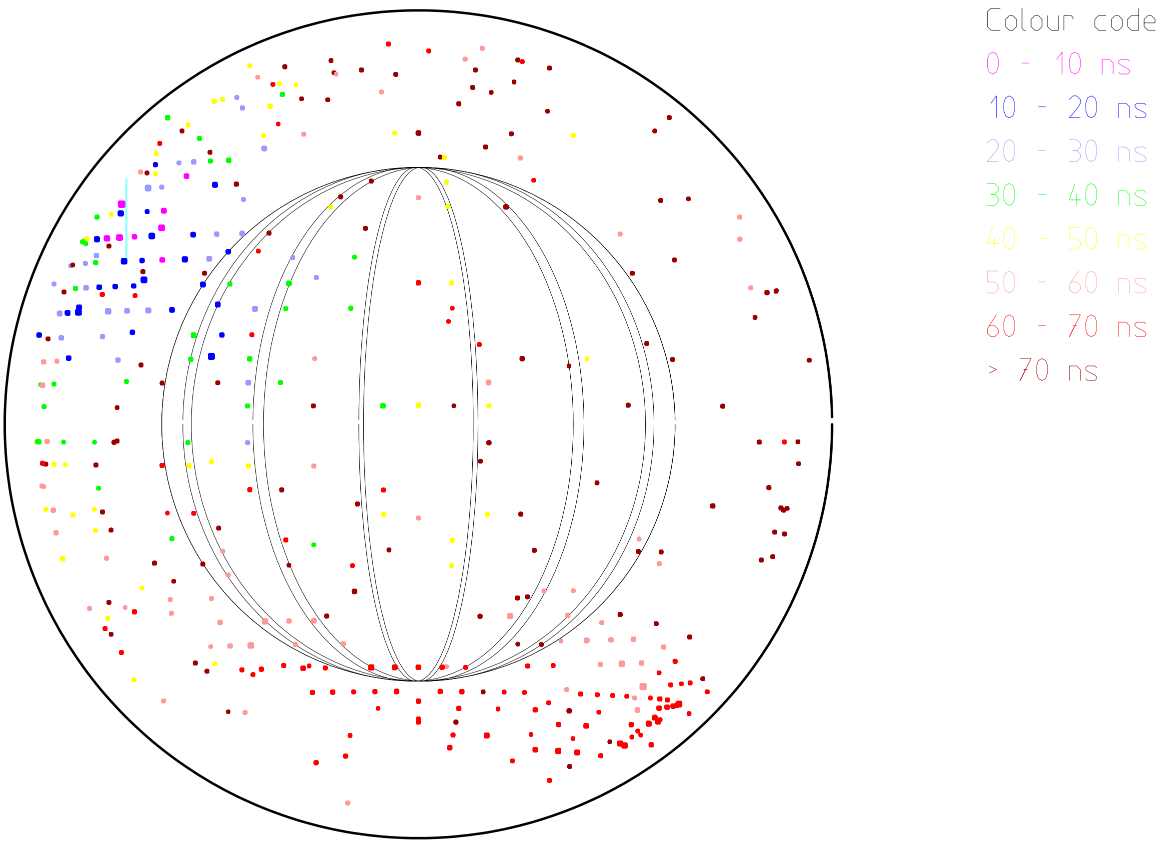

Figure 11: *Detector response on a muon (turquoise track) intersecting the buffer region of the Inner Detector. Every PM above threshold is depicted. The size scales with the pulse height, the colour with the timing of the first photon registered: blue corresponds to very fast photons, red spots to long time delay.*

scintillator with high efficiency, but suppress the detection probability for photons with the 'wrong' directionality. These tubes with light guides 'see' mainly the scintillator. Fig. 13 shows the acceptance curve, i.e. the photon collection efficiency, for point like events as a function of the distance to the center of the detector. Details of the light guides design can be found in [7].

Hence the photon yield for Cherenkov events is reduced in channels with light guides. Therefore the relative yield in tubes *without* light guides is higher for muon pulses. On the other hand, the relative yield in tubes *with* light guides for beta events occurring in the scintillator (e.g. neutrino candidates) is enhanced compared to those without light guides. Therefore, comparison in the photon yields between this two classes of PMs provides an additional tool for event separation.

The position of the tubes without light guides was optimized for recognition of muons which intersect the buffer region close to the surface of the steel sphere, because these events create pulse heights in the region of interest. Fig. 14 shows the fraction of the sum of photoelectrons in channels without light guides over the total sum for betas and for muons as well.

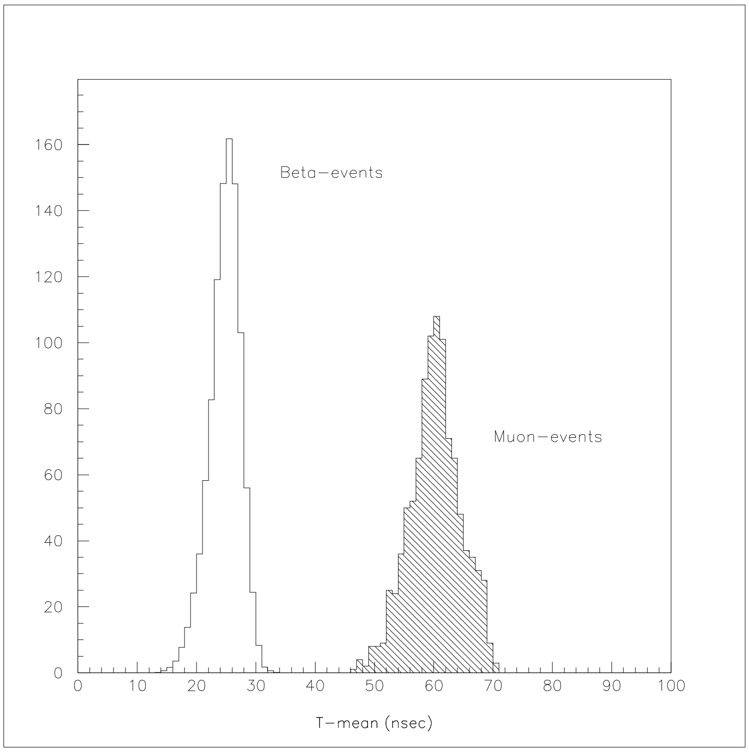

Figure 12: *Mean time distribution of beta-like events occuring inside the scintillator sphere, and muon events in the buffer region.*

The separation capability of this "fraction cut" is clearly demonstrated. A part of the muon signal comes from the scintillation process in the buffer. For wavelengths around 320nm the attenuation length in the buffer is at about 30cm. Therefore the detection efficiency for these photons is enhanced if the tubes without light guides are not pushed forward, allowing muon identification via this cut even for tracks very close to the steel surface. There is a shadowing effect for muons which have tracks in front of the photomultiplier, however this effect is small and only affects muons with very large pulse heights outside the neutrino window. In addition the high statistics of these events allows excellent muon identification via the timing as explained above. Fig. 15 shows the fraction cut for muons as function of the track distance to the center, clearly indicating the discrimination capability against betas even for muons close to the surface.

We conclude, that the optimized design of the ID should allow efficient muon identification. Both, the use of tubes without light guides as well as the analysis of the event timing contributes to the separation capability. Calculations showed, that both methods are quite robust against changes in parameter of the optical model. For complete changes in the buffer liquid and the scintillator (e.g. "PXE & water" solution) the calculations have not been completely finished. There is indication that both methods will work also under this conditions, however with somehow reduced efficiency.

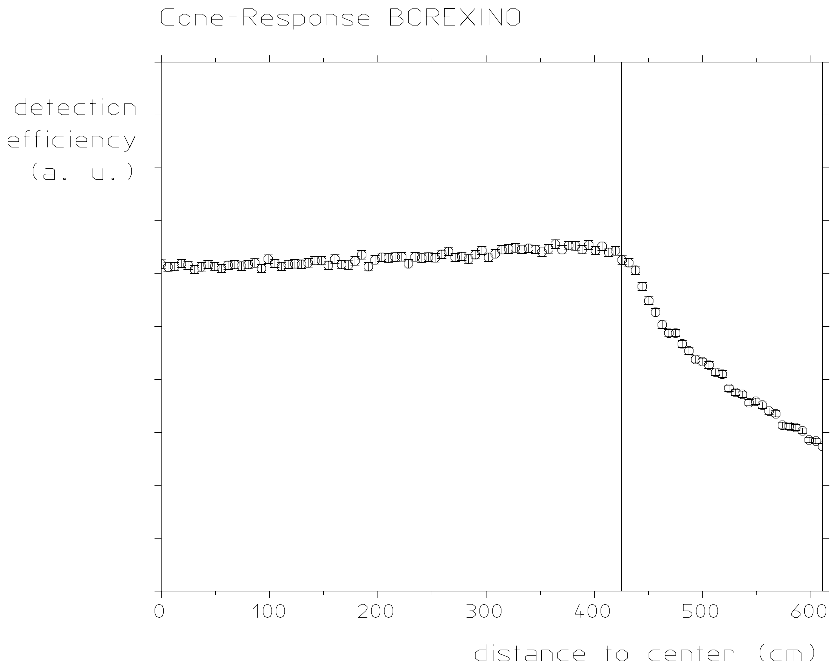

Figure 13: *Acceptance curve of Borexino light guides. High efficient photon collection with aluminum light guides (ca. 90% reflectivity) is established for beta-like events inside the inner vessel and drops at the border to the liquid buffer region.*

5.1 Rejection Efficiency of the ID

The rejection efficiencies to cosmic muons which intersect the ID are summarized in Tab. 6. Here the buffer liquid was assumed to be PC with the addition of a small amount of a quencher which reduces the scintillation output of PC by a factor of 10. The most promising candidate for such a quencher is dimethylphthalate (DMP). Out of 2240 PMs there are 1866 equipped with light guides. It was assumed, that all tubes are working.

method	accept. good events (%)	muon leak (%)
pulse height	≈ 100	< 14
pe-fraction	> 99	2.3
tmean	≈ 100	< 0.1

Table 6: *Remaining muon leak after applying criteria provided by the ID. Discussion on the rates see text.*

Only a fraction of at most 14% of muons intersecting the steel sphere create signals with pulse heights inside the neutrino window. Applying the "fraction cut" provided by the PMs without cones, and analyzing the mean time distribution of the signals more than 99% of the muons should be rejected while almost no loss in good events must be expected. The results remain robust under small changes in the optical model. For dramatic changes in the choice of scintillator and buffer liquid the calculations have not

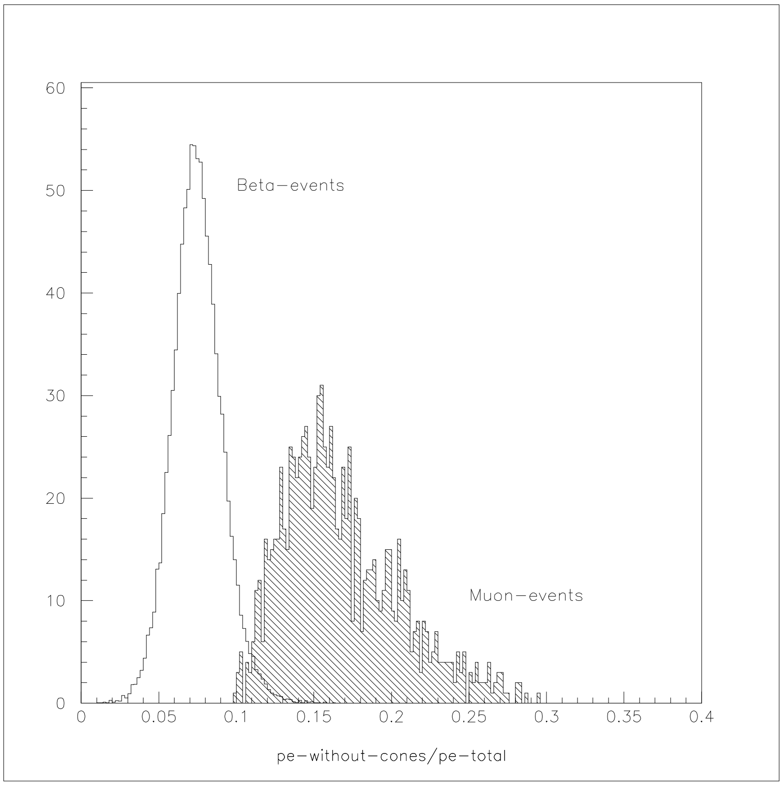

Figure 14: *Fraction of the sum of photoelectrons in channels without light guides over the total sum for beta events in the scintillator and for muons intersecting the buffer region.*

yet completed.

Under the assumption of a 50% PM failure the rejection factors are slightly reduced. However, also in this scenario the aimed rejection of 95% should be reached. Only in pathological situations where the PM failure is not distributed more or less homogeneously above the whole sphere a significant loss in the rejection power has to be expected.

6 Muon Induced Production of Radioisotopes

In addition to signal generation by Cherenkov photons of traversing muons, neutrino-like events can be created by the decay of cosmogenic produced radio-instable isotopes. Eventually underground production and decay will be in equilibrium. Depending on the life time of the nuclei, it can be correlated spatially and timely with the generating muon. Tab. 7 lists the relevant isotopes which are produced in a liquid scintillator target. It is noteworthy that the absence of heavier isotopes than ^{12}C limits the problem of long living activities.

	Isotopes	$t_{1/2}$	E_{max}
β^-	^{12}B	0.20 sec	13.4 MeV (β^-)
	^{11}Be	13.80 sec	11.5 MeV (β^-)
	^{11}Li	0.09 sec	20.8 MeV (β^-)
	^{9}Li	0.18 sec	13.6 MeV (β^-)
	^{8}Li	0.84 sec	16.0 MeV (β^-)
	^{8}He	0.12 sec	10.6 MeV (β^-)
	^{6}He	0.81 sec	3.5 MeV (β^-)
β^+, EC	^{11}C	20.38 min	0.99 MeV (β^+)
	^{10}C	19.30 sec	1.9 MeV (β^+) (+0.72 MeV γ)
	^{9}C	0.13 sec	16.0 MeV (β^+)
	^{8}B	0.77 sec	13.7 MeV (β^+)
	^{7}Be	53.3 days	0.478 MeV (γ)

Table 7: *Radioactive isotopes which are produced by muons and their secondary shower particles when passing through a scintillator target which consists of ^{12}C and ^{1}H dominantly. Of particular relevance for Borexino are the isotopes ^{7}Be,^{11}C, ^{10}C and ^{11}Be. Radio instable isotopes which emit $\beta-$neutron cascades as ^{8}He, ^{9}Li and ^{11}Li are important for anti-neutrino spectroscopy.*

Muon induced radioisotopes are important backgrounds in Borexino for several reasons: the decay products can generate signals

- in the ^{7}Be neutrino energy window (0.25-0.8 MeV), indistinguishable from ^{7}Be neutrino events;
- in the pep neutrino energy window (0.8 - 1.5 MeV), indistinguishable from pep neutrino events;
- in the high energy range relevant for ^{8}B neutrinos; here the isotope ^{11}Be is most relevant;
- in the energy range relevant for electron anti-neutrino detection; ^{8}He, ^{9}Li and ^{11}Li can emit $\beta-$neutron cascades mimicking the anti-neutrino ($\bar{\nu}_e$) tag [e^+ →(0.2 ms delay)+($n + p \rightarrow 2.2 MeV\gamma$)]. The muon correlated event sequence ($\mu \rightarrow e \rightarrow$

n) can be discriminated from $\bar{\nu}_e$ signals ($e^+ \rightarrow n$) by the characteristic triple coincidence, if the muon is recognized;

- in the energy window between 0.8 and about 3 MeV which is of importance in order to determine the residual background contributions of K, U and Th.

The production rates underground were not known precisely; from CTF measurements we found a neutron production rate of 0.3 neutrons per day and ton. The neutron rate can be taken as a gross estimate for the production rate of radioisotopes in Borexino. Hence one expects a production/decay rate of 100 events per day in 300 tons. Most of the isotopes have live times in the sub-sec scale. It is possible to discard these activities with a moderate loss of measuring time by imposing a veto cut subsequent to a muon signal in the off-line analysis. This, however, is not possible for ^{11}Be,^{11}C,^{10}C and ^{7}Be. Their life times are too long in order to veto the whole detector after every muon traversing the detector.

In the production of ^{11}C and ^{10}C from ^{12}C there are one or two neutrons emitted respectively which will be (delayed) captured by protons giving rise to a 2.2 MeV gamma. It is thinkable that the light C isotopes can be discarded on a one by one base defining a decay volume in the off-line analysis around the position of the neutron capture. The question of convection of ^{11}C has to be addressed in-situ in the Borexino detector.

6.1 Measurements at Cern (NA54)

A statistical subtraction of events generated by muon induced isotopes is possible only if the effective cross sections are known accurately. As the relevant numbers have not been measured yet, we performed a dedicated experiment (NA54) at the Cern muon beam in order to deduce the cross sections of interest.

The isotope production by muons and their secondaries $\mu(\&shower)+^{12}\mathrm{C}\rightarrow^{A}_{Z}\mathrm{X}$ has been studied experimentally in the frame of the NA54 experiment at Cern [13, 14]. Depending on the particular production mechanism, the contribution of the secondary particles can be dominating. For example, it has been observed that the production of ^{11}C increases by one order of magnitude in a saturated shower. There existed no precise data of the production of the isotopes of interest. The measurements at Cern were carried out with the objective to measure the effective cross sections for the production of light radio-instable isotopes and moreover, to measure the lateral activation profile, i.e. the probability that a particular isotope is produced at a given distance from the muon track. The latter is of relevance for example in the case that spatial spallation cuts will be applied in the Borexino data analysis.

Similar experimental conditions as encountered in the Borexino experiment were simulated in the Cern experiment. 240 cm of concrete followed by 200 cm of water was placed in front of the ^{12}C targets. The shower is built up in the concrete and water and reaches saturation after typically 1-2 m. Two energies, 100 and 190 GeV, were available during this period of measurements (mean energy in the LNGS is 280 GeV) and various muon intensities were selected. The maximal intensity available was a few 10^8 muons per spill of 2.4 sec duration at a frequency of 14.4 sec.

Depending on the decay mode of the produced isotopes different detection techniques were chosen. This comprises low-level gamma spectroscopy for ^{7}Be, $\beta - \gamma$ coincidence counting for ^{11}C and in-situ scintillation spectroscopy for short lived isotopes.

6.2 Activation Profile and Preliminary Results

Most of the isotopes could be identified and the cross sections are currently under evaluation. Only preliminary numbers are given in this report.

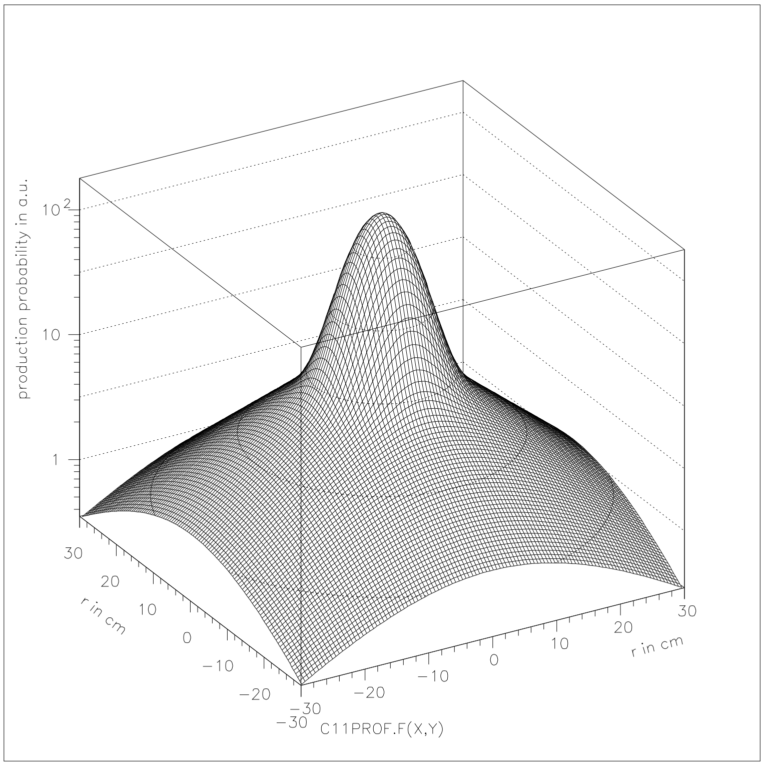

Figure 15: *Lateral distribution of ^{11}C production in muon induced showers. The activation profile, i.e. the probability of ^{11}C production at a distance from the center of the shower (muon track) is displayed.*

In Fig. 15 the lateral distribution of ^{11}C production is shown with respect to the muon trajectory. For illustration purpose, Fig. 17 depicts the decay of ^{11}Be, ^{8}Li and ^{8}B. Fig. 16 displays the composite curve of ^{8}B and ^{10}C.

Tab. 6.2 lists the measured cross sections. The missing entries in the table indicate that the values are still under evaluation. Tab. 6.2 gives the expected event rate in Borexino assuming an energy dependence of the cross section according $\sigma \propto E^{0.7}$ and a muon energy spectrum from Ref. [15]

The final results will be included in a later version of this report.

		100 GeV	190 GeV
β^-	$\sigma(^{12}\mathrm{B})$		
	$\sigma(^{11}\mathrm{Be})$		
	$\sigma(^{9}\mathrm{Li})$		
	$\sigma(^{8}\mathrm{Li})$		
	$\sigma(^{6}\mathrm{He})$		
β^+, EC	$\sigma(^{11}\mathrm{C})$	$605.9 \pm 10\%$	$942.2 \pm 10\%$
	$\sigma(^{10}\mathrm{C})$		
	$\sigma(^{9}\mathrm{C})$		
	$\sigma(^{8}\mathrm{B})$		
	$\sigma(^{7}\mathrm{Be})$	$126.5 \pm 10\%$	$230.0 \pm 10\%$

Table 8: *Measured cross sections σ in μb for the production of radio instable isotopes from ^{12}C at two muon energies. The data evaluation is currently under progress - hence missing entries - and the given values for ^{7}Be and ^{11}C are preliminary.*

β^-	$^{12}\mathrm{B}$	
	$^{11}\mathrm{Be}$	
	$^{9}\mathrm{Li}$	
	$^{8}\mathrm{Li}$	
	$^{6}\mathrm{He}$	
β^+, EC	$^{11}\mathrm{C}$	$13.0 \pm 10\%$
	$^{10}\mathrm{C}$	
	$^{9}\mathrm{C}$	
	$^{8}\mathrm{B}$	
	$^{7}\mathrm{Be}$	$3.0 \pm 10\%$

Table 9: *Rate of muon induced isotopes in Borexino at Gran Sasso in units events/day/100t. The blanks are currently under evaluation.*

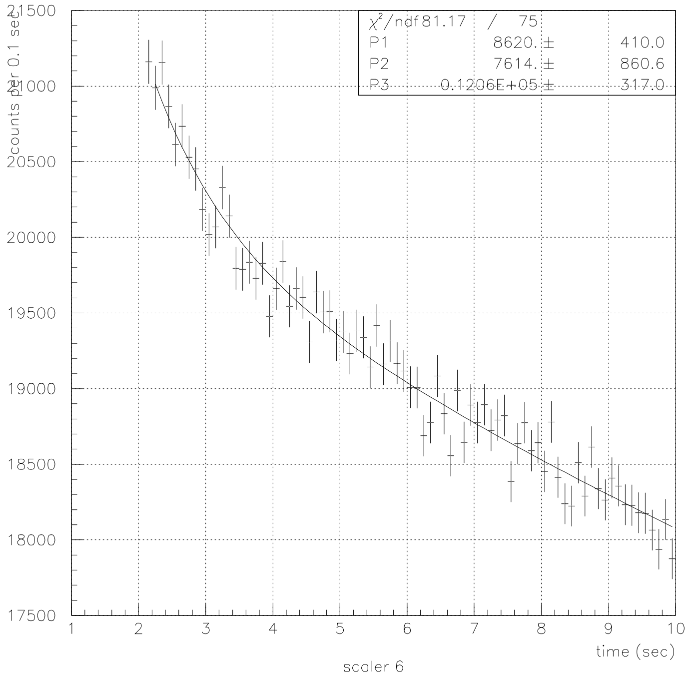

Figure 16: *composite decay curve of the* β^+ *decays of* ^8B ($t_{1/2}$ = 0.77 *sec*, E_{max} = 13.7 *MeV*) *and* ^{10}C ($t_{1/2} = 19.3$ *sec*, $E_{max} = 1.9$ *MeV*).

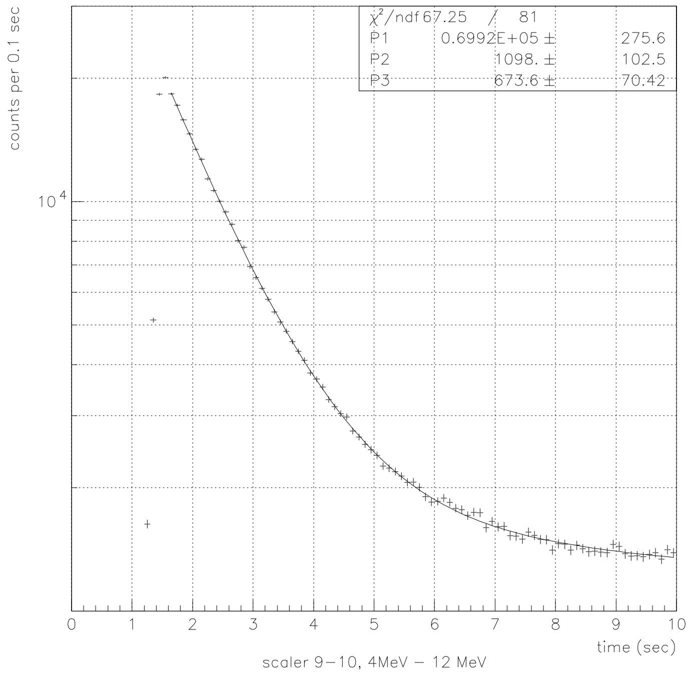

Figure 17: *The fast component of the decay curve is composed of the β decays of ^{11}Be ($t_{1/2}$ = 13.8 sec, E_{max} = 11.5 MeV) and ^{8}Li ($t_{1/2}$ = 0.84 sec, E_{max} = 16.0 MeV) and the slow component comes from the decay of ^{8}B ($t_{1/2}$ = 0.77 sec, E_{max} = 13.7 MeV).*

7 Manpower and Cost Estimates

The composition of the muon veto group in the Borexino collaboration is listed in Tab. 10 (january 1998).

MIT		
	M. Deutsch	Prof.
Princeton		
	M. Chen	Ass. Prof.
	R. Eisenstein	Prof.
TU-München		
	T. Hagner	PhD std.
	L. Oberauer	Ass. Prof.
	S. Schönert	postdoc
	K.H. Schuhbeck	engineer
	E. Seitz	techn.
	F. von Feilitzsch	Prof.

Table 10: *Institutes and persons involved in the muon identification working group of Borexino.*

Item	cost/channel	total costs
Photomultiplier	1770,-DM	709.000,-DM
Electronics	850,-DM	340.000,-DM
Cable, connectors	555,-DM	222.000,-DM
PM-base (encaps.)	345,-DM	138.000,-DM
Acrylic plates (OD)	293,-DM	59.000,-DM
Optical fiber (OD)	300,-DM	60.000,-DM
PM-support	100,-DM	40.000,-DM
Mu-metal	194,-DM	78.000,-DM
Support struct. tyvek		20.000,-DM
Tyvek material		10.000,-DM
Sum		1676.000,-DM

Table 11: *Estimated costs for items of the muon id system.*

Tab. 11 comprises the estimated costs for the muon identification system. It includes only capital investment. No overhead is taken into account.

The funding situation for the muon system is as follows:

- The german funding agency BMBF approved for **270.000,-DM** available from january 1998.

- In the frame of the Munich special research center "Particle Astrophysics" the german funding agency DFG approved for **340.000,-DM** available from january 1998.

- The Princeton group is asking for **600,000 US $**.

With the actual exchange rate (1.8 DM for 1 US $) the costs are covered by the foreseen total budget of 1690,000,-DM with almost negligible contingency. It should be stressed that the price of the PM was increasing by about 30% in the last year simply because the british sterling was becoming so expensive in this period (the company EMI producing our PMs is british).

8 Conclusions

Cosmic ray muons and their secondaries are an important source of background in Borexino. Signals are generated a) by Cherenkov and scintillation photons from traversing muons and shower particles and b) by muon induced radioisotopes. In order to measure solar ^{7}Be neutrinos it is imperative to recognize cosmic ray signals with an overall efficiency of about 1 false event in 10^4. This demanding requirement will be addressed by the Borexino Muon Identification System (MIS). It is based on the combined information obtained from the Outer Detector (OD), the Inner Detector (ID) and the off-line analysis. Their individual efficiencies will be calibrated mutually.

We have performed Monte Carlo studies of the performances of the different detector parts. A variety of off-line cuts have been examined and their viability could be demonstrated. The Monte Carlo analysis indicate that the required detection efficiencies will be met.

The effective cross sections for muon induced production of radio-instable isotopes were measured in a dedicated experiment (NA54) at the muon beam at Cern. From these measurements it is possible to predict accurately the event rate due to cosmogenic nuclei in Borexino. The results are still under evaluation and the final results will be reported at a later time.

8.1 Acknowledgement

Up to summer 1997 the Borexino working group on the muon identification system (MIS) consisted only of Martin Deutsch from MIT and the Munich team as listed in Tab. 7. We emphasize, that the basic aspects of MIS have been already described in the NSF-proposal of Martin. Now, after the optimization of the detector design which is described in this account, one can conclude that these basic ideas have been confirmed. We, the Munich group, gratefully appreciate all the discussions with Martin about this topic and about all other aspects of life in and outside of physics.

In addition we are indepted to Prof. Ecke Nolte and Bernhard Heisinger from the TU-München, who work in the field of cosmogenic background creation due to high energetic muons since a long time, and who included us so nicely in their famous NA54 experiment performed at the SPS at CERN. It also should be mentioned, that Roger von Hentig participated in the NA54-measurements in a very important manner and not only the muon group, but also the whole collaboration benefits from his expertise in low background techniques.

References

[1] R.S.Raghavan, *Phys. Rev. Letters 78, (1997) 3618*

[2] R. S. Raghavan, S. Schönert, S. Enomoto, J. Shirai, F. Suekane and A. Suzuki, *Phys. Rev. Letters 80, (1998) 635*

[3] C. Rothchild, M. Chen, P. Calaprice, *Geophys. Letters (1998)*, accepted for publication.

[4] S. Schönert, *Nucl. Phys.* **B**, *Proc. Suppl., TAUP97*, Gran Sasso, Italy, Sept. 1997, to be published

[5] G.Alimonti et al., BOREXINO collaboration, *Astr. Phys. J. (1997)*, accepted for publication

[6] G.Alimonti et al., BOREXINO collaboration, *Phys. Lett.* **B** *(1997)*, accepted for publication

[7] G.Alimonti et al., BOREXINO collaboration, *Nucl. Instr. Meth. (1997)*, accepted for publication

[8] T.Goldbrunner et al., *Journ. of Rad. Nucl. Chem., 216, (1997) 293*

[9] R. Claus *et al.*, *NIM* **A***261 (1987) 540-542*

[10] The Front-End Electronics of the Borexino detector, S. Vitale *et al.*, *Borex Report 97-xx-xx.*

[11] Feasibility studies of the geochemical solar neutrino experiment ^{205}Tl(ν_e,e)^{205}Pb. S. Neumaier et al., Z. Phys. A 340 (1991), 415-418

[12] The muon induced background in the GALLEX experiment. M. Cribier et al., Astroparticle Physics 6 (1997) 129-141.

[13] B. Heisinger, Doctorate thesis TU-München (1998)

[14] T. Hagner, R. v. Hentig, B. Heisinger, L. Oberauer, S. Schönert, F. v. Feilitzsch, *Muon induced production of radio-instable isotopes in scintillation detectors*, to be published (1998).

[15] P. Lipari and T. Stanev, *Phys. Rev.* **D** 44 (1991) 3543